ARTICLE

Tuning tRNA synthetase inhibition reveals parabolic induction of stress granules limited in size and RNA content

MAX BAYMILLER,[1,2,3] NOAH S. HELTON,[1,2] BENJAMIN DODD,[1,2] and STEPHANIE L. MOON[1,2]

[1]Department of Human Genetics, University of Michigan, Ann Arbor, Michigan 48109, USA
[2]Center for RNA Biomedicine, University of Michigan, Ann Arbor, Michigan 48109, USA
[3]Department of Molecular Biology and Biochemistry, Wesleyan University, Middletown, Connecticut 06459, USA

ABSTRACT

Translation elongation defects cause ribosome stalling and activate the integrated stress response (ISR). During the ISR, translation initiation suppression and ribosome runoff drive mRNA condensation into stress granules. However, the effects of partial translation elongation inhibition on stress granules are poorly defined. We demonstrate that intermediate levels of tRNA synthetase inhibitors activate the ISR and cause assembly of stress granules in a parabolic dose–response pattern. These stress granules are limited in size and number due to ribosome association with mRNAs. Assembly of stress granules by intermediate levels of the prolyl-tRNA synthetase inhibitor halofuginone requires the canonical stress granule scaffolding proteins G3BP1/2 and GCN2-mediated ISR activation. We performed a candidate-based comparative analysis of the composition of stress granules induced by intermediate levels of halofuginone or canonical stressors arsenite or thapsigargin. The stress granules induced by halofuginone, arsenite, or thapsigargin harbor polyadenylated RNA and the canonical stress granule proteins PABPC1, G3BP1, and UBAP2L. We observe stress- and transcript-specific differences in the localization of candidate RNA molecules to stress granules. These results demonstrate that partial translation elongation inhibition permits stress granule assembly through the balance of ISR activation and mRNA association with ribosomes, with implications for the stress response associated with amino acid or tRNA deficiency, therapeutic tRNA synthetase inhibition, or diseases associated with tRNA synthetase mutations.

Keywords: stress granules; tRNA synthetase; halofuginone; translation; translation elongation; integrated stress response

INTRODUCTION

The integrated stress response (ISR) is a conserved signaling pathway activated in response to physiological challenges including nutrient deprivation, toxic metalloid exposure, RNA damage, and ER stress. During the ISR, translation initiation is suppressed when stress-sensing kinases GCN2 (general control nonderepressible 2), HRI (heme regulated inhibitor), PKR (protein kinase R), or PERK (PKR-like endoplasmic reticulum kinase) phosphorylate the translation initiation factor eIF2α (Pakos-Zebrucka et al. 2016; Costa-Mattioli and Walter 2020). Inhibition of translation initiation by P-eIF2α promotes stress-induced gene expression (Young and Wek 2016) and drives the assembly of biomolecular condensates called stress granules (Kedersha et al. 2005). Stress granules are implicated in cellular stress resilience and form through multivalent RNA–RNA, RNA–protein, and protein–protein interactions, typically driven by G3BP1-mediated phase separation (Kedersha et al. 2016; Guillén-Boixet et al. 2020; Sanders et al. 2020; Yang et al. 2020). Stress granules are enriched in translationally repressed mRNAs and RNA binding proteins such as G3BP1 (G3BP stress granule assembly factor 1), PABPC1 (poly(A) binding protein), and UBAP2L (ubiquitin associated protein 2 like) (Kedersha et al. 2005; Khong et al. 2017; Moon et al. 2019). Stress granule formation depends on both translation initiation suppression and continued translation elongation, and the association of mRNAs with one or more ribosomes inhibits their assembly into stress granules (Kedersha et al. 2000, 2005; Mollet et al. 2008; Khong and Parker 2018; Moon et al. 2019, 2020; Helton et al. 2025). Thus, the release of mRNAs from ribosomes is critical for stress granule assembly during the ISR.

Translation elongation stresses (e.g., UV stress, amino acid deprivation, RNA damage, or loss of tRNA synthetase

Corresponding author: smslmoon@umich.edu
Handling editor: Eric Phizicky
Article is online at http://www.rnajournal.org/cgi/doi/10.1261/rna.080883.125. Freely available online through the *RNA* Open Access option.

activity) trigger the ISR via GCN2 by causing stalled ribosomes and/or uncharged tRNAs to accumulate (Wek et al. 1989; Dever et al. 1992; Dong et al. 2000; Keller et al. 2012; Darnell et al. 2018; Inglis et al. 2019; Wu et al. 2020; Stoneley et al. 2022; Misra et al. 2024; Zhou et al. 2025; Baymiller et al. 2026). However, under conditions of widespread ribosome stalling, stress granule assembly would require mRNA release from stalled ribosomes through resumed elongation, ribosome-associated quality control (RQC), or other ribosome release pathways. Indeed, conflicting findings in the literature suggest that stress granules can assemble upon UV stress (Moutaoufik et al. 2014; Ying and Khaperskyy 2020; Zhou et al. 2024), while other translation elongation stress conditions do not cause stress granule formation (Arimoto et al. 2008; Baymiller et al. 2026) or lead to aberrant stress granule–like assemblies (Aulas et al. 2018; Pietras et al. 2022). These studies suggest that the degree of translation elongation inhibition could correspond with the degree of impaired assembly and composition of stress granules. We recently demonstrated that despite ISR activation, stalled ribosomes persist on mRNAs and stress granule assembly is inhibited by saturating concentrations of tRNA synthetase inhibitors or amino acid deprivation (Baymiller et al. 2026). The results of our prior study suggest that stalled, uncollided ribosomes are not rescued, and mRNAs remain trapped within polysomes during robust tRNA synthetase inhibition or amino acid depletion. However, the effects of partial translation elongation suppression, which may represent many physiological stress conditions, on stress granule assembly remain unclear.

tRNA synthetase inhibitors provide tractable tools to study translation elongation stress, as they block translation elongation and activate the ISR in a dose-dependent fashion (Keller et al. 2012; Misra et al. 2021, 2024; Pitera et al. 2022; Rai et al. 2024). Aminoacyl-tRNA synthetases are essential genes that mediate tRNA charging with amino acids to facilitate polypeptide chain formation during translation elongation. There is increasing interest in the cellular response to halofuginone as a model for tRNA synthetase defects and amino acid deprivation stress (Pitera et al. 2022; Misra et al. 2024; Zhou et al. 2025; Baymiller et al. 2026). Halofuginone and borrelidin, which inhibit proline and threonine tRNA charging by glutamyl-prolyl tRNA synthetase (EPRS1) and threonyl-tRNA synthetase, respectively, are of therapeutic interest as immunosuppressants and for treatment of fibrosis, scleroderma, parasitic infections, cancer, and diabetes (Pines and Nagler 1998; Sundrud et al. 2009; Habibi et al. 2012; Sidhu et al. 2015; Rai et al. 2024). Additionally, mutations in tRNA synthetases are associated with peripheral neuropathies such as Charcot–Marie–Tooth disease (CMT) and multisystem disorders (Antonellis et al. 2003; Kuo and Antonellis 2020). The ISR is activated in motor neurons and contributes to pathogenesis in mouse models of *Gars* mutant CMT (Spaulding et al. 2021; Zuko et al. 2021), and patient fibroblasts with compound heterozygous *EPRS1* mutations hyperactivate the ISR during ER stress (Jin et al. 2021). Unlike widely used translation inhibitors that directly bind the ribosome, tRNA synthetase inhibitors recapitulate physiologically relevant ribosome stalling that occurs with amino acid deprivation or loss-of-function tRNA synthetase mutations (Jin et al. 2021, 2023; Misra et al. 2021, 2024; Spaulding et al. 2021; Pitera et al. 2022; Zhou et al. 2025). Given their dose-dependent effects on translation elongation and ISR activation, tRNA synthetase inhibitors provide a tractable experimental tool to systematically investigate how varying degrees of biologically relevant translation elongation stress impact stress granule assembly.

In this study, we examine how varying levels of tRNA synthetase inhibitors affect stress granule formation and composition. We observe a unique, parabolic pattern of stress granule assembly during tRNA synthetase inhibition: stress granules form at low-to-intermediate, but not very low or high, levels of halofuginone or borrelidin. Puromycin restores stress granule assembly during tRNA synthetase inhibition, indicating that stress granule assembly is limited by mRNAs trapped in polysomes during elongation stress. These stress granules are dependent on the canonical stress granule scaffolding proteins G3BP1/2 and translation initiation suppression via the GCN2-activated ISR pathway to assemble. Canonical stress granule proteins are present within stress granules induced by intermediate doses of halofuginone, but partition within them to a lesser extent compared to typical ISR-inducing stressors thapsigargin and arsenite. Further, comparative RNA localization analysis demonstrates stress- and transcript-specific differences in stress granule RNA composition. Halofuginone causes smaller stress granules and generally results in fewer RNAs localizing to stress granules than thapsigargin and arsenite. These results establish that low-to-intermediate levels of tRNA synthetase inhibitors cause GCN2-dependent stress granule assembly that is limited by mRNA retention within ribosomes.

RESULTS

tRNA synthetase inhibitors activate the ISR in a dose-dependent manner

To evaluate the dose-dependence of ISR activation during tRNA synthetase inhibition, we measured levels of phosphorylated eIF2α (P-eIF2α) in cells treated with halofuginone, borrelidin, or the canonical ISR inducers arsenite and thapsigargin. We used human osteosarcoma U-2 OS cells for these experiments, which are routinely used for ribosome-associated quality control, ISR, and stress granule studies (Kedersha et al. 2005; Khong et al. 2017; Moon et al. 2019; Wu et al. 2020; Goldman et al. 2021;

Snieckute et al. 2023; Helton et al. 2025). As expected, 1 h treatments with arsenite (25–250 μM) (Fig. 1A) or thapsigargin (0.04–1 μM) (Fig. 1B) induced P-eIF2α in a dose-dependent manner. Halofuginone also induced a dose-dependent increase in P-eIF2α from 0.2 to 20 μM (Fig. 1C), consistent with prior work (Keller et al. 2012; Pitera et al. 2022; Rai et al. 2024).

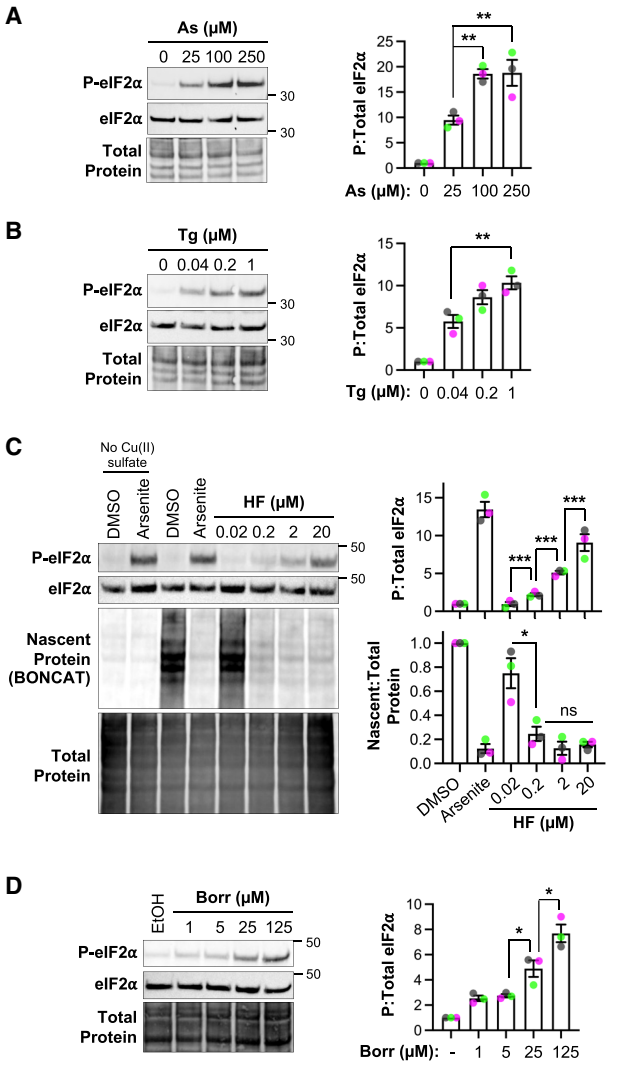

FIGURE 1. tRNA synthetase inhibition induces dose-dependent eIF2α phosphorylation similar to canonical stressors. Western blot of P-eIF2α and total eIF2α from U-2 OS cells treated with arsenite (As) at 25–250 μM for 1 h (*A*) or thapsigargin (Tg) at 0.04–1 μM for 1 h (*B*). (*C*) P-eIF2α and total eIF2α western blot with nascent (BONCAT) and total protein from U-2 OS cells treated with DMSO (0.2%) control, arsenite (500 μM, 30 min), or halofuginone (HF) at 0.02–20 μM for 4 h. No copper controls are shown at *left*. (*D*) Western blot of U-2 OS cells treated with borrelidin (borr; 1–125 μM for 4 h) or ethanol (EtOH) carrier. Representative western blots with total protein loading controls and molecular weights in kDa shown at *left* with quantification of $n = 3$ independent replicates with averages ± SEM and replicate values shown as green, gray, and pink points at *right*. Significance assessed with ordinary one-way ANOVA and Tukey's multiple comparisons tests with (*) $P < 0.05$, (**) $P < 0.01$, (***) $P < 0.005$.

We applied bioorthogonal noncanonical amino acid tagging (BONCAT) (Dieterich et al. 2006) to measure the degree of bulk translation suppression by halofuginone. BONCAT revealed a significant reduction in protein synthesis between 0.02 and 0.2 μM halofuginone, with the amount of nascent proteins generated in halofuginone-treated cells comparable to that of high concentration arsenite stress despite lower levels of P-eIF2α (Fig. 1C). In contrast to P-eIF2α levels, however, no further decrease in translation activity occurred with increasing halofuginone concentrations. These results suggest that halofuginone potently inhibits translation at the levels of initiation via P-eIF2α and elongation via decreased charged $tRNA^{Pro}$. Inhibition of threonyl-tRNA charging using increasing levels of borrelidin caused a similar increase in P-eIF2α levels over a ∼100-fold concentration range (1–125 μM) (Fig. 1D). Therefore, like canonical stressors, tRNA synthetase inhibitors cause a dose-dependent increase in ISR activation and suppress translation.

Low-to-intermediate levels of tRNA synthetase inhibitors induce stress granules limited by mRNA association with ribosomes

We next assessed whether stress granules assemble in a dose-dependent fashion upon tRNA synthetase inhibition by visualizing GFP-G3BP1 stably expressed in U-2 OS cells (Burke et al. 2020). We found that treating cells with increasing levels of canonical stressors arsenite or thapsigargin increased the percentage of cells with stress granules, with ∼100% of cells exhibiting stress granules at the highest concentrations (Fig. 2A,B). In contrast, cells treated with halofuginone or borrelidin for 4 h show a parabolic pattern of stress granule assembly, as the highest percentage of cells with stress granules occurred at intermediate concentrations (2 μM halofuginone or 25 μM borrelidin) (Fig. 2C, D). Specifically, treatment with 0.2 μM halofuginone caused small GFP-G3BP1 foci in 35% ± 4.0% of cells, which increased approximately twofold to 65% ± 5.4% at 2 μM halofuginone (Fig. 2C). The 4 h treatment time was selected based on live cell imaging experiments, which demonstrated stress granules begin to assemble ∼2 h after halofuginone addition and approach steady-state at ∼4 h (Supplemental Movie S1). Similar results were observed with borrelidin (Fig. 2D). Therefore, stress granules are only induced at low-to-intermediate concentrations of tRNA synthetase inhibitors despite causing a dose-dependent increase in ISR activation.

Two pieces of evidence suggest that mRNA association with stalled ribosomes limits stress granule assembly during halofuginone or borrelidin treatment. First, puromycin restored stress granule assembly in cells treated with tRNA synthetase inhibitors (Fig. 2). Puromycin is a peptidyl-tRNA mimic that displaces nascent proteins from ribosomes and releases ribosomes from mRNAs (Azzam and Algranati

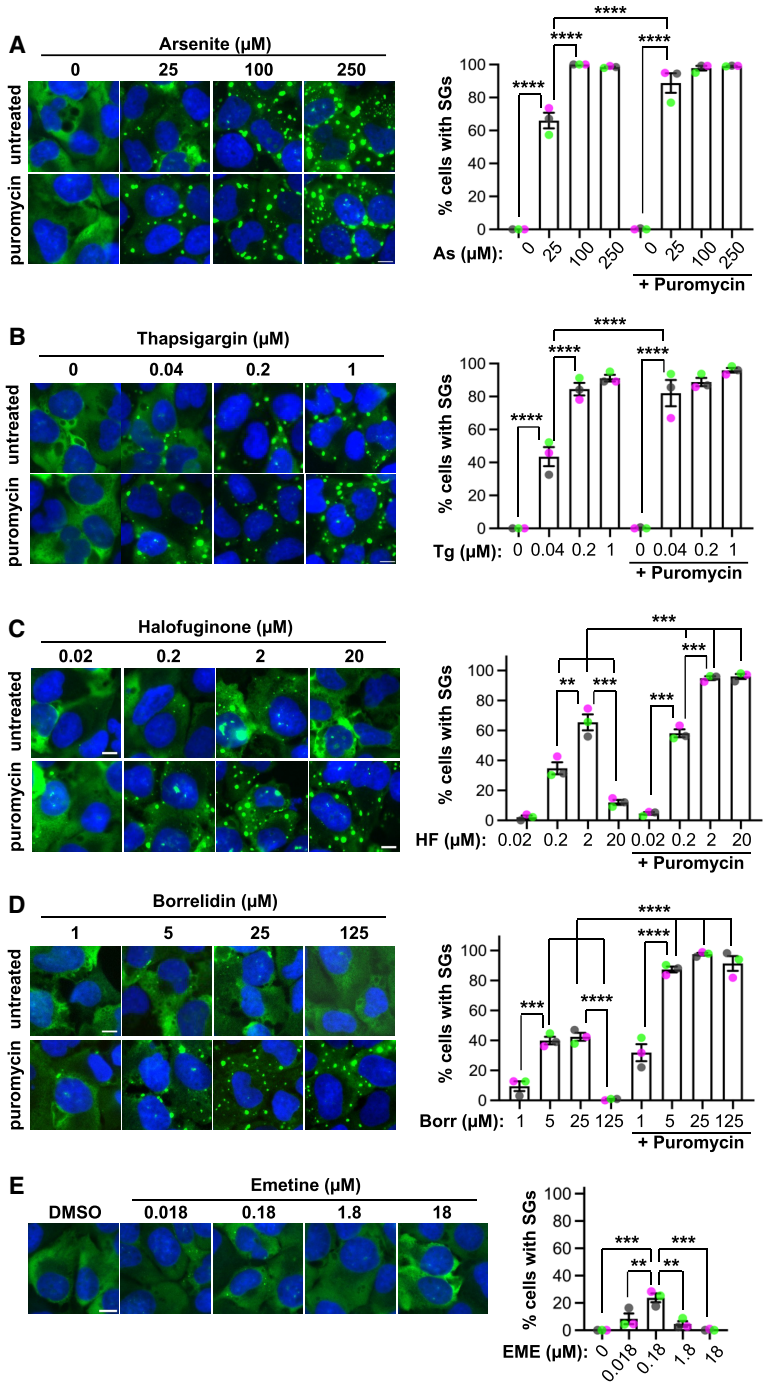

FIGURE 2. Low-to-intermediate concentrations of tRNA synthetase inhibitors induce stress granules limited by mRNA association with ribosomes. (*A*) U-2 OS cells expressing GFP-G3BP1 (green) were treated with arsenite (25–250 μM, "As," 1 h) in the presence or absence of puromycin (10 μg/mL); nuclei stained with Hoechst (blue). (*B*) Cells were treated with thapsigargin (0.04–1 μM, "Tg," 1 h) in the presence or absence of puromycin (10 μg/mL). (*C*) Cells were treated with halofuginone (0.02–20 μM, "HF," 4 h), with or without puromycin (10 μg/mL) for the last 30 min. (*D*) Cells were treated with borrelidin (1–125 μM, "Borr," 4 h) in the presence or absence of puromycin (10 μg/mL) for the last 30 min. (*E*) Cells were treated with DMSO control or emetine (0.018–18 μM, "EME," 45 min). Representative images (*left*) are from $n = 3$ independent replicates, and the average ± SEM of the percentage of cells with stress granules with green, gray, and pink points showing each replicate value is shown at *right*. Scale bars, 10 μm. Significance determined with ordinary one-way ANOVA followed by Tukey's multiple comparisons tests; (**) $P < 0.01$, (***) $P < 0.005$, (****) $P < 0.001$.

1973; Enam et al. 2020). We therefore assessed whether puromycin treatment would increase stress granule assembly in cells treated with varying doses of arsenite, thapsigargin, halofuginone, or borrelidin.

We observed that a 30 min pulse of puromycin significantly increased the number of cells with stress granules during treatment with halofuginone or borrelidin, with most cells exhibiting stress granules at the highest concentrations of each inhibitor (Fig. 2C, D). Specifically, puromycin caused ~100% of cells to form stress granules at 2 and 20 μM halofuginone, a 1.4- and 8.0-fold increase compared to cells treated with halofuginone alone (Fig. 2C). Live cell imaging demonstrated that puromycin increases stress granule assembly within ~5 min in cells treated with halofuginone (Supplemental Movie S2). Similar 2.2-, 2.3-, and 130-fold increases were observed in the percentage of cells with stress granules in cells treated with 5, 25, and 125 μM borrelidin, respectively (Fig. 2D). Interestingly, puromycin also increased the percentage of cells with stress granules in cells cotreated with the lowest levels of arsenite (25 μM) (Fig. 2A) or thapsigargin (0.04 μM) (Fig. 2B), suggesting some mRNAs are still associated with ribosomes in these low stress concentrations. A 30 min puromycin pulse did not induce stress granule assembly in unstressed cells (Fig. 2A,B) or cause eIF2α phosphorylation (Baymiller et al. 2026), suggesting puromycin does not further activate the ISR to induce stress granules upon tRNA synthetase inhibition. In line with the results of our prior study (Baymiller et al. 2026), restoration of stress granule assembly with puromycin suggests that mRNAs that remain associated with ribosomes limit stress granule formation during tRNA synthetase inhibition.

Second, we observed a similar non-monotonic pattern of stress granule assembly in cells treated with the direct ribosome translocation inhibitor emetine as in cells treated with tRNA synthetase inhibitors. Emetine inhibits

translation elongation and activates the ISR via ribosome collisions at intermediate concentrations (e.g., 180 nM) (Sinha et al. 2020; Wu et al. 2020; Stoneley et al. 2022; Baymiller et al. 2026). Interestingly, we observed that 24.6% ± 1.4% of cells treated with an intermediate (180 nM) emetine concentration have small stress granules, but few if any cells exhibit stress granules at low (18 nM) or high (1.8 or 18 µM) emetine concentrations (Fig. 2E). It is likely that a combination of low P-eIF2α levels and the essentially irreversible inhibition of translation elongation by emetine (Grollman 1968) limits stress granule formation in this context. Therefore, translation elongation stressors cause a distinct parabolic stress granule assembly phenotype suggesting that a balance between translational inhibition and elongation dictates conditions where stress granule assembly is permissive.

Stress granule assembly requires GCN2 activation upon tRNA synthetase inhibition

We next established the role of GCN2 in activating the ISR during tRNA synthetase inhibition. GCN2 is activated by collided, stalled ribosomes and uncharged tRNAs. We first verified that proline supplementation led to halofuginone-induced stress granule disassembly. We observed that proline supplementation (5 mM) significantly reduced P-eIF2α levels (Fig. 3A) and caused stress granule disassembly within 1 h (Fig. 3B). These results demonstrate that halofuginone specifically activates the ISR and causes stress granule assembly due to the inhibition of prolyl-tRNA synthetase activity.

Next, we tested the hypothesis that the ISR is required for stress granule assembly during halofuginone treatment in two ways. First, we cotreated stressed cells with the ISR inhibitor ISRIB, which blocks the effects of P-eIF2α on translation inhibition during stress by increasing eIF2B activity (Sidrauski et al. 2013; Tsai et al. 2018). We observed that ISRIB inhibits stress granules from forming upon low-level halofuginone treatment, as halofuginone caused stress granules in 31% ± 6.6% cells, but only 2.0% ± 0.3% cells exhibited stress granules in the presence of ISRIB (Fig. 3C). ISRIB significantly reduced, but did not completely inhibit, stress granule assembly in cells cotreated with halofuginone and puromycin (Fig. 3C). As expected, ISRIB significantly reduced the number of cells with stress granules during arsenite or DTT stress (Fig. 3C; Sidrauski et al. 2015). Therefore, the ISR is required for halofuginone-induced stress granule assembly.

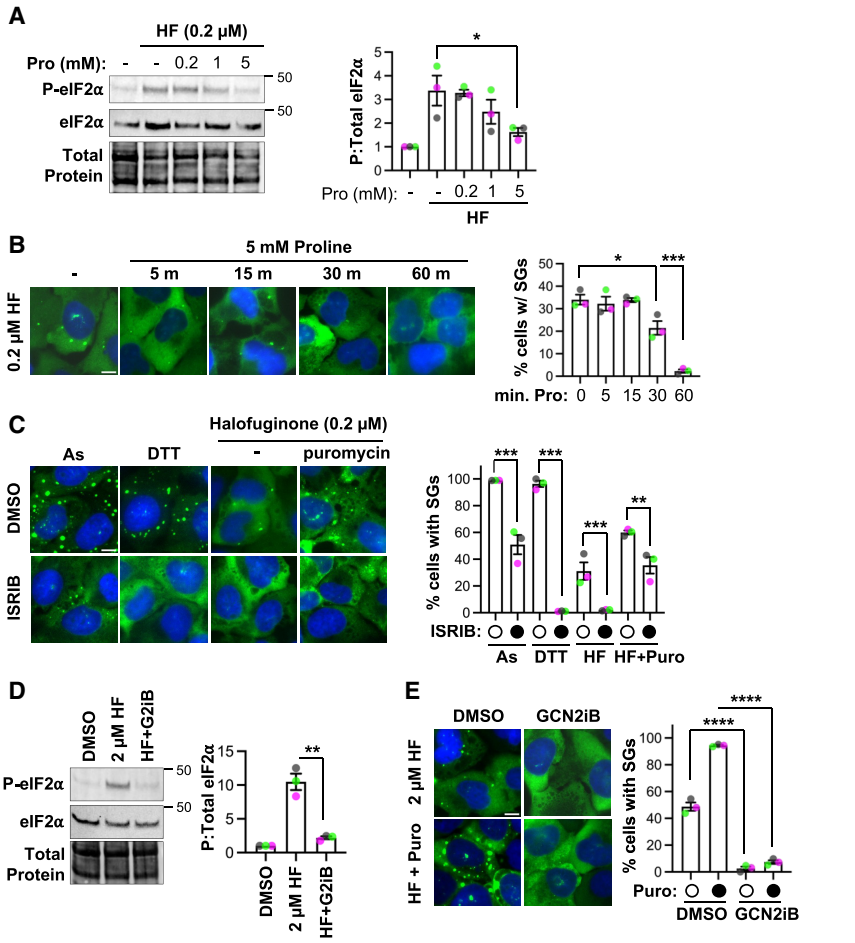

FIGURE 3. Stress granule assembly during halofuginone treatment requires the GCN2-mediated ISR. (*A*) P-eIF2α and total eIF2α western blot of cells treated with halofuginone (0.2 µM, "HF") and proline (0–5 mM) for 4 h. (*B*) U-2 OS cells expressing GFP-G3BP1 (green) were treated with halofuginone (0.2 µM, 4 h) with proline (5 mM) added for 5–60 min; cells were fixed and nuclei stained with Hoechst (blue). (*C*) Stress granules (GFP-G3BP1) detected in cells treated with DMSO carrier or ISRIB (1 µM) for 4 h, stressed with arsenite (0.25 mM) or DTT (2 mM) added for the last 30 min, or cotreated with halofuginone (0.2 µM) for 4 h, with or without puromycin (10 µg/mL) added for the last 30 min. (*D*) Western blot of P-eIF2α and total eIF2α from cells treated with DMSO control, or halofuginone (2 µM) for 4 h with DMSO carrier or GCN2iB (5 µM, "HF + G2iB"). (*E*) Stress granules (GFP-G3BP1) in cells treated as in *D*, with or without puromycin (10 µg/mL) added for the last 30 min. Representative images (at *left*) shown from $n = 3$ independent replicates, and quantifications reported as average ± SEM with green, gray, and pink points representing the values from each replicate (at *right*). Significance assessed with ordinary one-way ANOVA followed by Tukey's multiple comparisons tests with (*) $P < 0.05$, (**) $P < 0.01$, (***) $P < 0.005$, (****) $P < 0.001$. Scale bars, 10 µm. Molecular weights (kDa) are shown for each western blot.

Second, we evaluated whether the eIF2α kinase GCN2, which is activated by halofuginone (Keller et al. 2012; Pitera et al. 2022; Misra et al. 2024), is required for stress granules during tRNA synthetase inhibition. We treated cells with GCN2iB, a small molecule inhibitor of GCN2, and evaluated P-eIF2α and the percentage of cells that form stress granules in cells treated with halofuginone and/or puromycin. Prior studies demonstrated *GCN2* depletion inhibits eIF2α phosphorylation during halofuginone treatment (Pitera et al. 2022; Misra et al. 2024), and halofuginone induces ribosome collisions that activate GCN2 (Zhou et al. 2025; Baymiller et al. 2026). We confirmed that GCN2iB significantly reduces P-eIF2α levels upon halofuginone treatment (Fig. 3D). Additionally, we observed that GCN2iB significantly reduced the percent of cells with stress granules caused by halofuginone in the presence or absence of puromycin (Fig. 3E). Therefore, GCN2 activity is required for stress granule formation upon treatment with intermediate levels of halofuginone.

Comparative analysis of protein and RNA assembly into stress granules across stressors

We next compared the protein and RNA composition of stress granules induced by tRNA synthetase inhibition or typical ISR-inducing stressors arsenite or thapsigargin by probing for canonical stress granule markers. We first assessed whether G3BP1 and paralog G3BP2 (G3BP stress granule assembly factor 1 and 2) are required for stress granules induced by intermediate levels of halofuginone. We treated wild-type or *G3BP1/2* knockout cells (Kedersha et al. 2016) with arsenite, thapsigargin, halofuginone, or halofuginone and puromycin, and measured stress granule assembly using immunofluorescence microscopy for PABPC1, which is typically observed in stress granules. We observed that stress granules do not form in the absence of G3BP1/2 in any condition (Fig. 4A). These data demonstrate that halofuginone-induced stress granules harbor PABPC1 and require G3BP1/2 to assemble, and are thus similar to stress granules caused by typical ISR-inducing stresses.

We then determined whether other typical stress granule proteins and polyadenylated RNA assemble into canonical stress- or halofuginone-induced stress granules in the presence or absence of puromycin. We performed immunofluorescence microscopy for G3BP1 and UBAP2L (ubiquitin-associated protein 2-like) and fluorescence in situ hybridization (FISH) with oligo(dT) probes in stressed cells in the presence or absence of puromycin. As anticipated, bulk polyadenylated RNA, G3BP1, and UBAP2L colocalized in stress granules in cells treated with arsenite or thapsigargin in the presence or absence of puromycin (Fig. 4B). Cells treated with intermediate levels of halofuginone also exhibited stress granules that contain poly(A)$^+$ RNA, G3BP1, and UBAP2L, which was unaffected by puromycin (Fig. 4C). As expected, untreated cells in the presence or absence of puromycin did not harbor foci of polyadenylated RNA, G3BP1, or UBAP2L (Fig. 4D). Therefore, halofuginone-induced stress granules contain RNA and RNA-binding proteins, similar to arsenite- or thapsigargin-induced stress granules.

We evaluated the partitioning of G3BP1, UBAP2L, and polyadenylated RNA into stress granules under conditions when mRNAs were associated with ribosomes or released from ribosomes by puromycin cotreatment during halofuginone, arsenite, or thapsigargin stress. We measured the fraction of each component inside and outside stress granules to derive a partitioning coefficient in stressed cells in the presence or absence of puromycin. Generally, the partitioning coefficients of polyadenylated RNA, G3BP1, and UBAP2L were lower in halofuginone-treated cells compared to arsenite or thapsigargin treatments (Fig. 5A–C). This result is consistent with the idea that halofuginone limits mRNA release from ribosomes by inhibiting translation elongation. We observed that puromycin generally increased the partitioning of polyadenylated RNA, G3BP1, and UBAP2L in cells treated with halofuginone, and also increased their partitioning during arsenite or thapsigargin stress (Fig. 5A–C), suggesting that ribosome association limits RNA and RNA-binding protein condensation in all tested conditions. While the number of stress granules per cell was not significantly different across stresses (Fig. 5D), stress granules were significantly smaller in halofuginone-treated cells compared to arsenite- or thapsigargin-treated cells (Fig. 5E). These results could indicate that halofuginone inhibits stress granule growth or fusion to a greater extent than stress granule nucleation compared to arsenite or thapsigargin. The number of stress granules per cell was significantly increased with puromycin in halofuginone and thapsigargin, but not in arsenite, stresses (Fig. 5D). Stress granule size was not significantly increased with puromycin in any stress (Fig. 5E). Together, these results provide additional evidence that freeing mRNAs from polysomes generally increases the condensation of protein and RNA components of stress granules.

We next evaluated whether specific transcripts had reduced localization to stress granules during treatment with intermediate levels of halofuginone compared to thapsigargin and arsenite stress, and were similarly sensitive to puromycin in their localization to stress granules across stresses. We examined the localization of the long noncoding RNA *NORAD*, two long mRNAs that are enriched in stress granules during arsenite stress, *AHNAK* and *DYNC1H1*, and the shorter mRNA that is largely excluded from stress granules *GAPDH* (Khong et al. 2017). We reasoned that *NORAD* would serve as a general marker of RNA condensation as it is recruited to stress granules but is not translated. We treated cells expressing GFP-G3BP1 with halofuginone (2 μM for 4 h), thapsigargin

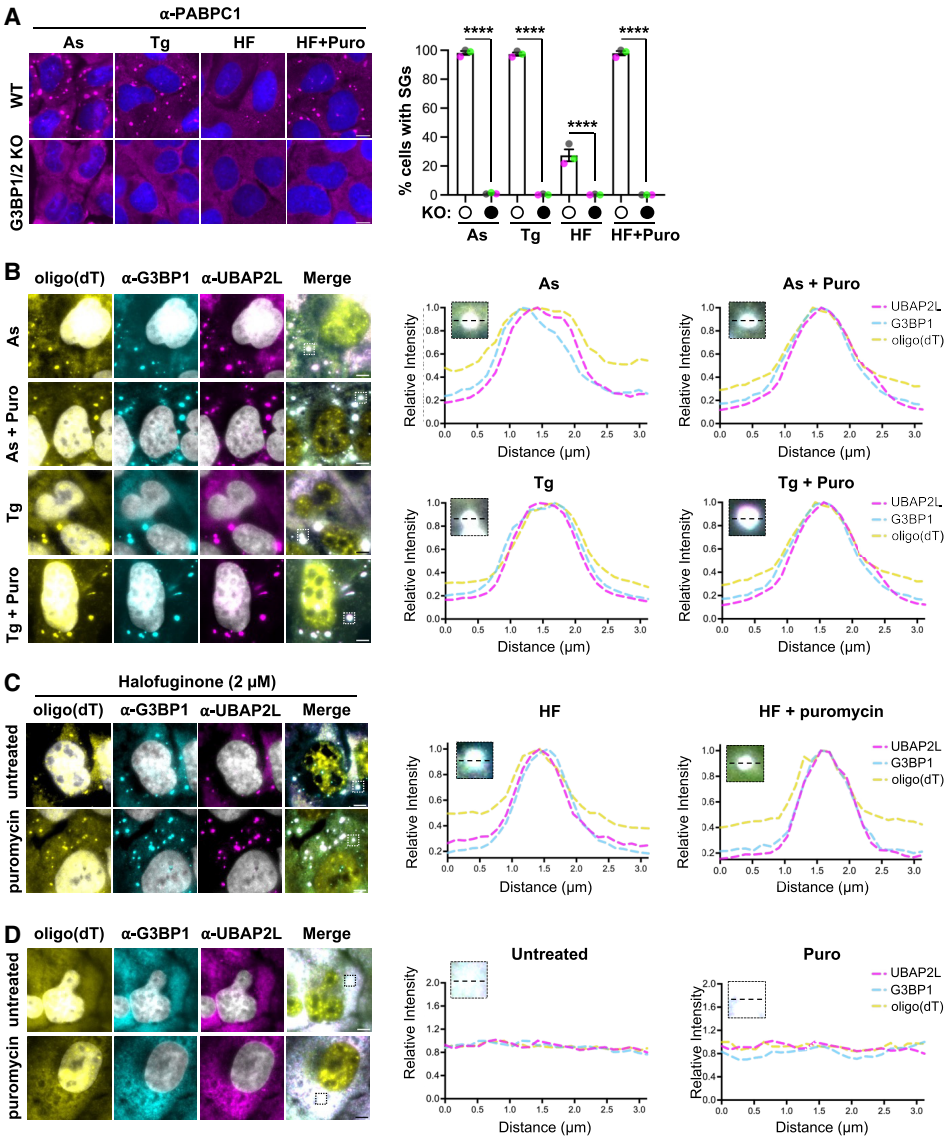

FIGURE 4. Halofuginone-induced stress granules require *G3BP1/2* and contain canonical stress granule markers. (*A*) Stress granules (PABPC1 immunofluorescence; magenta) in wild-type or *G3BP1/2* knockout U-2 OS cells treated with arsenite (250 µM, "As," 1 h), thapsigargin (1 µM, "Tg," 1 h), or halofuginone (2 µM, "HF," 4 h) with or without puromycin (10 µg/mL) for the last 30 min. Nuclei stained with Hoechst (blue). Average percentage of cells with stress granules ± SEM with green, gray, and pink points representing the value from each replicate shown at *right*. Significance assessed with ordinary one-way ANOVA followed by Tukey's multiple comparisons test with (****) $P < 0.001$. (*B*) Representative images (*left*) of stress granule markers [polyadenylated RNA detected with oligo(dT) FISH, or G3BP1 or UBAP2L by immunofluorescence] in U-2 OS cells treated with arsenite (25 µM) or thapsigargin (0.04 µM) with or without puromycin (10 µg/mL). G3BP1 in cyan, UBAP2L in magenta, poly(A)$^+$ RNA in yellow, and nuclei stained with Hoechst (gray). At *right*: Colocalization of stress granule markers (plot profile traces; peak for each channel set to 1) in a representative stress granule for each condition. (*C*) Stress granule markers in U-2 OS cells treated with halofuginone (2 µM, 4 h) with or without puromycin (10 µg/mL) during the last 30 min as in *B*. (*D*) Localization of poly(A)$^+$ RNA, G3BP1, or UBAP2L as in *B* and *C* in unstressed U-2 OS cells in the presence or absence of puromycin (10 µg/mL, 1 h). All results represent $n = 3$ independent replicates. Scale bars, 5 µm.

(0.04 µM for 1 h), or arsenite (25 µM for 1 h) and performed single-molecule FISH (smFISH) for *NORAD*, *AHNAK*, *DYNC1H1*, or *GAPDH*. We used a modified Big-FISH pipeline to determine the percent RNA in stress granules and in the cytoplasm in individual cells (Supplemental Fig. S1; Imbert et al. 2022; Helton et al. 2025).

We observed stress- and transcript-specific differences in RNA localization to stress granules. As anticipated based on past work (Khong et al. 2017; Khong and Parker 2018; Moon et al. 2019), substantially more *AHNAK*, *DYNC1H1*, and *NORAD* RNA molecules localized to stress granules compared to *GAPDH* molecules during arsenite stress

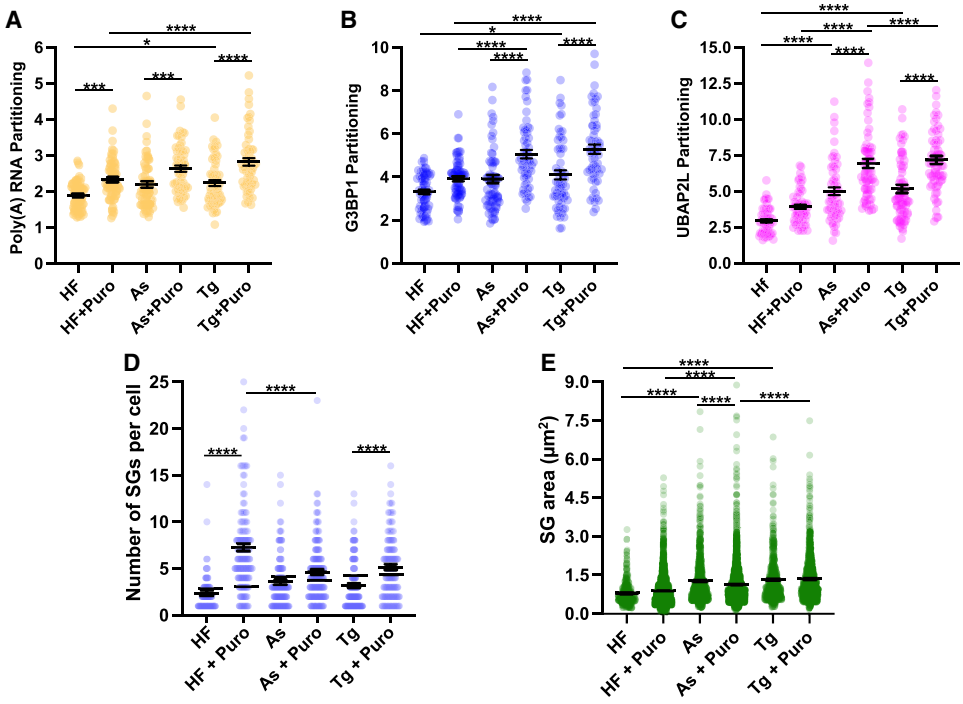

FIGURE 5. Comparative analysis of candidate stress granule properties in cells treated with halofuginone, arsenite, or thapsigargin in the presence or absence of puromycin. Partitioning coefficients of polyadenylated RNA (*A*), G3BP1 (*B*), or UBAP2L (*C*) from FISH/immunofluorescence images shown in Figure 4 ($n = 60$ cells). Cells were treated with halofuginone (2 µM, 4 h) with or without puromycin (10 µg/mL) added during the last 30 min or arsenite (25 µM, 1 h) or thapsigargin (0.04 µM, 1 h) with or without puromycin (10 µg/mL). Results are from three to four frames per replicate per condition from three independent experiments. (*D*) Number of stress granules per cell in cells treated as in *A*–*C*. Stress granules (UBAP2L staining) within 5 µm of the nuclear boundary were quantified. (*E*) Stress granule area (UBAP2L staining, within 5 µm of nuclear boundary) was determined. One-way ANOVA with Tukey HSD tests were done to assess significance with (*) $P < 0.05$, (***) $P < 0.005$, (****) $P < 0.001$.

(Fig. 6A,B). On average, the percentage of all analyzed RNAs localized to stress granules was lower in halofuginone-treated cells compared to arsenite-stressed cells (Fig. 6A,B). However, while *NORAD* and *GAPDH* localized to a similar extent to thapsigargin- and arsenite-induced stress granules, *DYNC1H1* and *AHNAK* were also significantly reduced in stress granules in thapsigargin stress compared to arsenite stress (Fig. 6A,B). We observed that puromycin treatment increased the localization of all RNAs to stress granules on average regardless of the stressor. For example, only 20% ± 1.3% of *AHNAK* or 21% ± 0.3% of *NORAD* were present in stress granules in cells treated with halofuginone, and puromycin significantly increased their partitioning in stress granules to 59% ± 2.7% and 56% ± 4.4%, respectively (Fig. 6A). However, puromycin generally had the least impact on RNA localization to stress granules during arsenite stress (Fig. 6A,B). It is possible that because arsenite stress (25 µM) causes approximately twofold higher P-eIF2α levels compared to thapsigargin stress (0.04 µM), translation initiation is suppressed more during arsenite stress. The reduced *NORAD* localization to halofuginone-induced stress granules compared to arsenite or thapsigargin stress is consistent with overall reduced RNA condensation in this context, consistent with decreased stress granule size. As observed in canonical stress treatments shown here and as previously described (Khong and Parker 2018; Helton et al. 2025), these results indicate that ribosome association with RNAs limits the localization of candidate RNA molecules to stress granules during halofuginone treatment.

DISCUSSION

In this study, we compared the RNA and protein composition of stress granules induced by low-to-intermediate levels of tRNA synthetase inhibitors to those induced by canonical stressors arsenite and thapsigargin. The assembly of stress granules peaks at intermediate doses of halofuginone or borrelidin, which are translation elongation inhibitors that activate the ISR, or emetine. Halofuginone-induced stress granules require the ISR via GCN2 activation and G3BP1/2 to form, and addition of puromycin increases their assembly. These data indicate that stress granule assembly during tRNA synthetase inhibition requires the ISR but is limited by retention of mRNAs within polysomes. The stress granules induced by halofuginone harbor canonical stress granule markers including polyadenylated RNA, G3BP1, PABPC1, and UBAP2L.

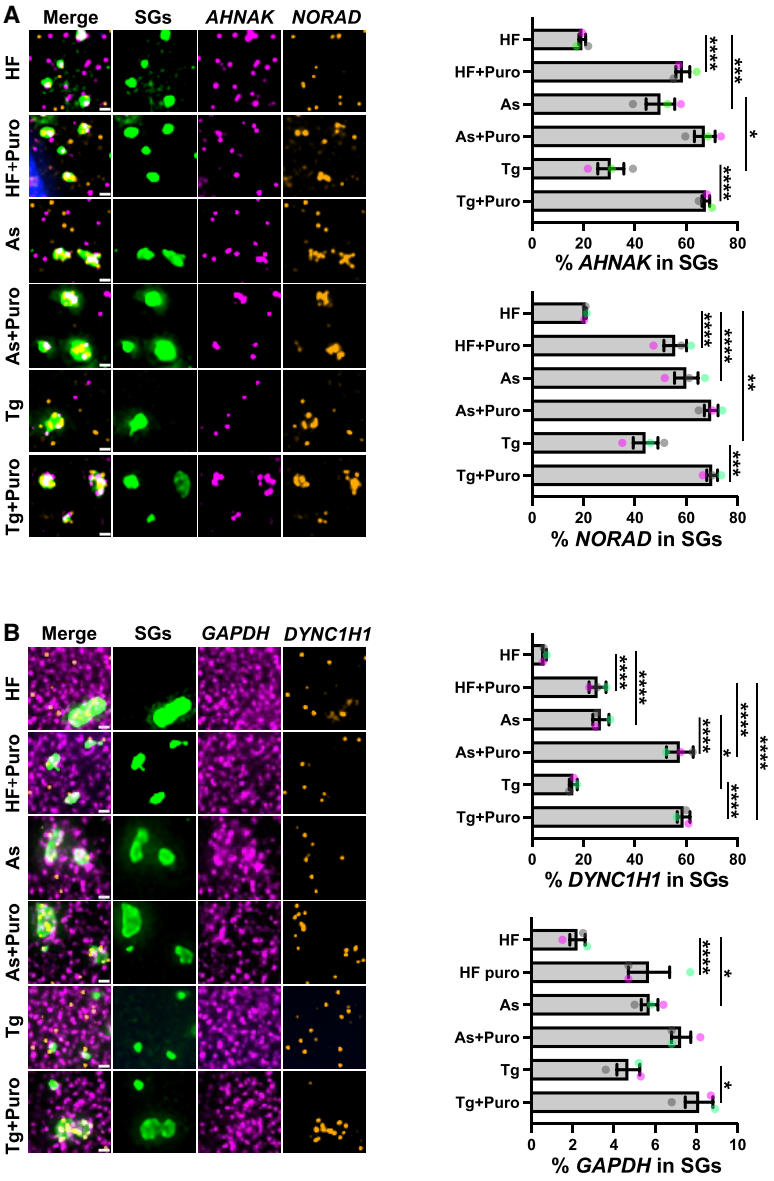

FIGURE 6. Comparative analysis of RNA localization to stress granules during halofuginone, arsenite, or thapsigargin stresses in the presence or absence of puromycin using a candidate approach. U-2 OS cells expressing GFP-G3BP1 (green) were treated with arsenite (25 µM, "As," 1 h) or thapsigargin (0.04 µM, "Tg," 1 h) in the presence or absence of puromycin (10 µg/mL), or halofuginone (2 µM, "HF," 4 h) with or without puromycin (10 µg/mL) for the last 30 min and smFISH performed. (*A*) *AHNAK* (magenta) and *NORAD* (gold) were probed in the same cells. (*B*) *GAPDH* (magenta) and *DYNC1H1* (gold) were probed in the same cells. For each panel, representative images are shown at *left*; at *right*: quantification of the average ± SEM percent RNA localization in stress granules from $n = 3$ independent experiments (15 cells per replicate) with the average from each replicate shown as green, gray, and pink points. Scale bars, 1 µm. One-way ANOVA with Tukey HSD tests were done to assess significance with (*) $P < 0.05$, (**) $P < 0.01$; (***) $P < 0.005$, (****) $P < 0.001$.

However, stress granules induced by halofuginone are smaller, generally have lower partitioning of RNA-binding proteins into them, and exhibit fewer candidate RNA molecules localized to them than those induced by arsenite or thapsigargin. These data together demonstrate that low-to-intermediate levels of tRNA synthetase inhibitors can trigger the assembly of stress granules that harbor canonical stress granule components but show distinct assembly kinetics.

One implication of our work is that the balance between translation initiation suppression and continued translation elongation dictates whether or not stress granules will form during stress (Fig. 7). We demonstrate that ISR activation is required for stress granules induced by low-to-intermediate concentrations of tRNA synthetase inhibitors using ISRIB or GCN2 inhibitors. Further, we observed a parabolic induction of stress granules, which form at low-to-intermediate, but not very low or high concentrations of tRNA synthetase inhibitors. The assembly of stress granules is restored with puromycin in cells treated with halofuginone or borrelidin, suggesting that mRNAs that remain associated with ribosomes limit stress granule assembly in these contexts. We recently demonstrated that amino acid deprivation, which results in the accumulation of uncharged tRNAs, also activates the ISR without inducing stress granule assembly (Baymiller et al. 2026). It is not clear how ribosomes persist in their association with mRNAs upon tRNA synthetase inhibition, but our previous work suggests failure of RQC pathways to recognize or clear uncollided stalled ribosomes (Baymiller et al. 2026). However, the requirement of VCP and other RQC factors in releasing some mRNA molecules from ribosomes during arsenite or heat stress suggests that there are translation quality control pathways that mediate mRNA localization to stress granules (Moon et al. 2020). Together with our prior study demonstrating that mRNA association with as few as one ribosome blocks stress granule assembly (Helton et al. 2025), these data demonstrate that ISR activation and mRNA release from ribosomes are required for stress granule formation during translation elongation stress. These findings reveal that stress granules integrate signals from translation initiation and elongation, and indicate the relative rate of elongation through their size and RNA composition.

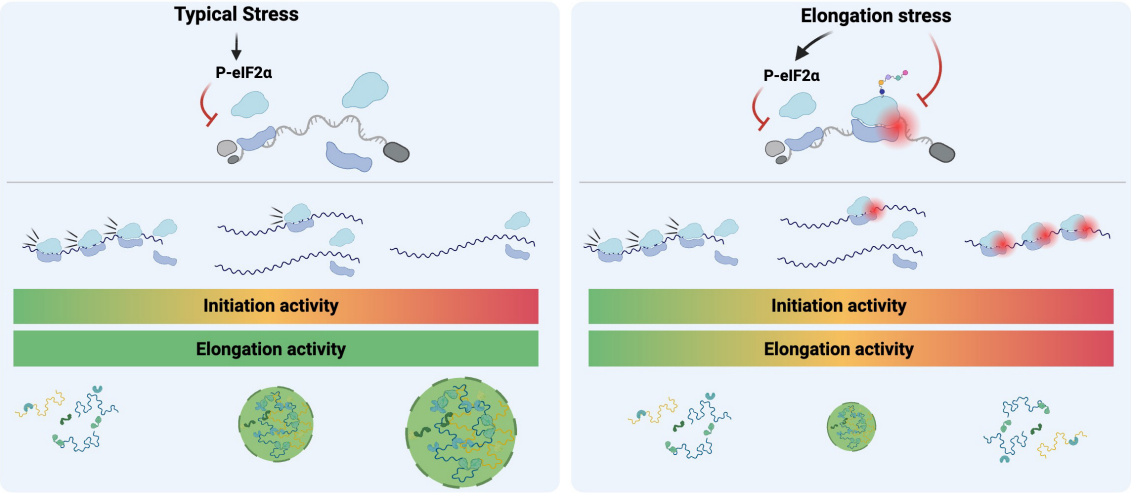

FIGURE 7. Model depicting stress granule assembly as a result of translation initiation inhibition and translation elongation activity. Typical stresses (e.g., arsenite, thapsigargin) cause translation initiation suppression via eIF2α phosphorylation, and ribosome runoff drives stress granule assembly (*left*). Elongation stresses (e.g., tRNA synthetase inhibition) also induce eIF2α phosphorylation but inhibit translation elongation, leading to a parabolic dose–response pattern of stress granule assembly.

A second implication of this research is that stress context can impact the RNA composition of stress granules. We observed that halofuginone generally caused reduced RNA recruitment to stress granules, and induced smaller stress granules than arsenite or thapsigargin. These results are consistent with the idea that the translation elongation inhibition caused by halofuginone reduces mRNA condensation into stress granules. However, comparative smFISH analyses demonstrate that stress granules induced by thapsigargin also harbor fewer candidate RNA molecules than those induced by arsenite stress. Because the noncoding RNA *NORAD* is also reduced in stress granules upon halofuginone treatment compared to other stresses, halofuginone appears to globally limit RNA condensation. Furthermore, the addition of puromycin generally increases RNA assembly into stress granules regardless of stress conditions. While it is possible that *NORAD* interacts with ribosomes, the observed increase in *NORAD* partitioning into stress granules upon puromycin addition is likely due to the general increase in RNA condensation. Prior studies also reported a similar reduction in *NORAD* localization to stress granules upon cycloheximide (Khong and Parker 2018) or harringtonine (Helton et al. 2025) treatment. Although these results are in line with the model that ribosome association inhibits mRNA localization to stress granules, our analyses were limited. We selected transcripts that span a wide range of enrichment in stress granules to provide an initial framework for evaluating the impacts of tRNA synthetase inhibition on RNA condensation. Future experiments should perform larger-scale analyses with additional controls to comprehensively assess the impacts of translation elongation defects on stress granule composition.

A third implication of this study is that impaired stress granule assembly due to mRNA association with ribosomes could potentially occur in genetic diseases associated with mutations in tRNA synthetases. Variants in aminoacyl-tRNA synthetase genes are associated with the dominant peripheral neuropathy Charcot–Marie–Tooth disease and recessive multisystem disease phenotypes (Antonellis et al. 2003; Kuo and Antonellis 2020). Because tRNA synthetases are essential genes, the residual tRNA synthetase activity in disease contexts may be analogous to partial suppression of tRNA synthetase activity with low levels of inhibitors. Indeed, mouse models of peripheral neuropathy associated with glycyl- or tyrosyl-tRNA synthetases exhibit ISR activation in α motor neurons in the spinal cord (Spaulding et al. 2021; Zuko et al. 2021). The ISR appears to be maladaptive in these contexts, as tRNA overexpression rescues neuropathy while reducing ISR activation (Zuko et al. 2021), and ISR inhibition improves neuropathy phenotypes (Spaulding et al. 2021). However, constitutive ISR activation is not observed in primary fibroblasts from patients with *EPRS1* loss-of-function mutations, suggesting tissue- and/or cell-type-specific effects (Kuo and Antonellis 2020; Jin et al. 2021, 2023). It is possible that the ISR pathway is disrupted by translation elongation defects associated with tRNA synthetase mutations that could contribute to altered stress-induced gene expression (Pitera et al. 2022) and stress granule assembly. However, additional experiments must be done to determine if and how acute tRNA synthetase treatments mimic disease-relevant stress granule phenotypes. Direct testing of stress granules in patient-derived cells or animal models of tRNA synthetase-associated diseases would need to be done to determine whether the altered stress granule phenotypes we observe

with acute tRNA synthetase inhibitor treatments are relevant to chronic disease states.

Our study establishes that translation elongation inhibitors that activate the ISR cause distinct stress granule assembly kinetics compared to other ISR-inducing stresses that only inhibit translation initiation. The parabolic dose–response of stress granule assembly during translation elongation stress reflects competition between translation initiation and elongation suppression in mediating stress granule assembly through mRNA availability for condensation. The stress granules induced by prolyl-tRNA synthetase inhibition contain typical stress granule markers, but are smaller and generally exhibit reduced RNA localization to them compared to canonical stressors. These findings have potential implications for understanding the stress response during therapeutic tRNA synthetase inhibition and in genetic diseases that impact tRNA synthetase function.

MATERIALS AND METHODS

Cell culture and treatments

U-2 OS cells stably expressing EGFP-G3BP1 via lentivirus transduction were described previously (Burke et al. 2020) and kindly shared by James Burke and Roy Parker. Wild-type U-2 OS cells were obtained from ATCC (HTB-96). *G3BP1/2* knockout cells were used with permission from Paul Anderson and shared by Roy Parker (Kedersha et al. 2016). Cells were cultured in high glucose DMEM with glutamine and pyruvate supplemented with 9% FB essence (FBE; Avantor), 2 mM GlutaMAX (Gibco), and 1% penicillin–streptomycin in a 5% CO_2 37°C incubator. Stress treatments and other compounds were used as follows unless otherwise indicated: sodium arsenite (Ricca Chemical Company) at 25–500 µM for 30–60 min, thapsigargin (AG Scientific) in DMSO at 0.04–1 µM for 60 min, halofuginone (MedChemExpress [MCE] HY-N1584) in DMSO at 0.02–20 µM for 4 h, borrelidin (MCE HY-N6742) in ethanol at 1–125 µM for 4 h, ISRIB (MCE) in DMSO at 1 µM for 4 h, dithiothreitol (DTT) at 2 mM for 1 h, 10 µg/mL puromycin (Gold Biosciences) for 30 min, and GCN2iB (MCE HY-112654) in DMSO at 10 µM for 4 h.

Western blotting

Cells were treated as indicated, washed in PBS, and then 1× RIPA buffer with Halt protease and phosphatase inhibitor cocktail (Fisher Scientific PI78443) and benzonase (Fisher 70-746-4) was added directly to the plate. Lysates were supplemented with 4× Bolt LDS Sample Buffer (Fisher B0007) and Bolt Reducing agent (Fisher BT0005), heated at 70°C for 10 min, and then loaded onto a Bolt 4%–12% Bis-Tris gel (Invitrogen NW04120) and electrophoresed in Tris-MES-SDS running buffer (VWR 76371-730). Proteins were transferred to a PVDF membrane, and the membrane was stained with Total Protein Q reagent (Azure Biosystems 2225) and imaged. The membrane was then blocked in TBST with 5% nonfat dry milk and blotted as indicated. Antibodies used are listed in Table 1. All images were collected with an Azure Biosystems c600 Imaging System. Band intensities were quantified using ImageJ (Schindelin et al. 2012).

Bioorthogonal noncanonical amino acid tagging (BONCAT)

Cells were treated with stressors as indicated, and 10 min prior to collection were switched to methionine-free DMEM with 4 mM azidohomoalanine (AHA) for noncanonical amino acid incorporation. Cells were then lysed in 1× RIPA buffer with Halt protease and phosphatase inhibitor cocktail (Fisher Scientific PI78443) and benzonase (Fisher 70-746-4), and the Click-&-Go kit (Vector Laboratories CCT-1262) with Alexa 488 Alkyne (Invitrogen A10267) used for fluorescent labeling of the nascent proteins. No copper control reactions were done in parallel for DMSO or arsenite-treated conditions. Western blotting was performed as above, with the clicked fluorophore imaged on the membrane before total protein staining. Each lane was quantified with ImageJ, and the BONCAT intensity values were obtained by subtracting the background in the DMSO-treated no copper control reaction and reported as a ratio to the total protein signal.

TABLE 1. Antibodies used in this study

Antibody target (label)	Manufacturer	Catalog #	Dilution (method)
eIF2α	Santa Cruz	133132	1:1000 (western)
G3BP1 (CoraLite 488)	Proteintech	21004924	1:200 (IF)
PABPC1	Proteintech	66809	1:100 (IF)
Phospho-eIF2α	Abcam	ab32157	1:1000 (western)
UBAP2L	Cell Signaling Technology	40199S	1:200 (IF)
Mouse IgG (Alexa Fluor 568)	Invitrogen	A11011	1:1000 (IF)
Mouse IgG (DyLight 800)	Thermo Fisher Scientific	35521	1:5000 (western)
Rabbit IgG (Alexa Fluor 647)	Invitrogen	A21244	1:1000 (IF)
Rabbit IgG (DyLight 680)	Thermo Fisher Scientific	35568	1:5000 (western)

Fluorescence microscopy

For stress granule imaging, EGFP-G3BP1 U-2 OS cells were grown in glass-bottom 96 well plates, treated as indicated, and then fixed for 10 min with 4% paraformaldehyde (PFA) in PBS. For imaging of fluorescent proteins only, fixed cells were washed in PBS once, incubated in PBS with NucBlue Live Cell Stain (Invitrogen R37605) for 30 min at room temperature, and then rinsed in PBS before imaging. Images were collected on an EVOS M5000 fluorescence microscope (Invitrogen) using a 40× objective, and the percentage of cells with stress granules quantified from two frames per condition from $n = 3$ independent replicates manually using the Cell Counter plugin in ImageJ (Schindelin et al. 2012).

For quantification of stress granule sizes, number per cell, linescans, and partitioning coefficients, wild-type U-2 OS cells imaged via immunofluorescence and oligo(dT) FISH (see protocol below) were used. Partitioning coefficients were calculated by manually selecting a circular region of interest (ROI) within a stress granule in ImageJ, and taking the ratio of fluorescence intensity inside of it compared to an ROI of the same area in the adjacent cytoplasm. For area and numbers of stress granules, the UBAP2L channel was used to train a model in the Biodock AI software platform (www.biodock.ai) to detect stress granules, and this model was run on three to four frames per treatment from each of three independent biological replicates.

For live cell microscopy, media was exchanged to FluoroBrite (Gibco A1896701) supplemented with FBE and GlutaMAX 1 h before treatment, and epifluorescence imaging was performed with a 40× objective on a Nikon Eclipse Ti2 microscope equipped with a Lumencor Spectra III light engine, Andor Life 888 EMCCD camera, and Tokai Hit stage top incubator system set to 5% CO_2 and 37°C. Statistical tests indicated in the figure legends were done using either GraphPad Prism or R stats V4.4.2.

Single-molecule fluorescence in situ hybridization (smFISH) and immunofluorescence (IF)

FISH and smFISH were performed essentially as described in Khong et al. (2017) and Helton et al. (2025). Cells were grown and fixed in 4% PFA as above, followed by permeabilization in 0.1% Triton X-100 with 0.2 U/µL of RiboLock RNase inhibitor (Thermo Scientific EO0382). For detection of stress granule markers, cells were then incubated with primary antibodies (Table 1) diluted in PBS with 0.2 U/µL of RiboLock RNase inhibitor at room temperature for 1 h, washed 2×, and then incubated for 45 min with fluorescent secondary antibodies followed by three 5 min washes in PBS and a second fixation in 4% PFA for 10 min. Either after permeabilization (smFISH only) or the second fixation following antibody treatment (smFISH + IF), cells were then incubated in wash buffer A (10% formamide in nuclease-free 2× SSC) for 5 min, then placed in hybridization buffer (10% dextran sulfate, 10% formamide in 2× SSC) with probes to the indicated transcripts or Cy3-labeled oligo(dT) (Integrated DNA Technologies—IDT) at 37°C for 16–20 h. Hybridization buffer was removed, and each well incubated with wash buffer A with NucBlue Live Cell staining reagent (Invitrogen R37605) for 30 min at 37°C, followed by an additional 30 min in wash buffer A. Wash buffer A was replaced with wash buffer B (2× SSC), and samples were then imaged using HILO microscopy using a 100× objective of a custom Nikon Eclipse Ti2 microscope equipped with a GATACA Systems iLas2 total internal reflection by taking 11 Z stacks 0.2 µm apart. Representative images were deconvolved using a Richardson–Lucy algorithm in Nikon Elements and displayed as maximum intensity projections.

Preparation of smFISH probes was performed via a protocol adapted from Gaspar et al. (2017) as described in Helton et al. (2025). A tiled set of DNA probes complementary to a region of the transcript of interest was designed using the Stellaris Probe Designer from BioSearch Technologies, and these oligonucleotides were obtained from IDT and pooled. Probe sequences were reported in Helton et al. (2025), Moon et al. (2020), and Khong and Parker (2018). Pooled probes were then incubated with terminal deoxynucleotidyl transferase (Thermo Scientific EP0161) in a reaction containing dideoxy-UTP labeled with ATTO 565 or 646 dyes (Jenna Biosciences) at 37°C for 16–24 h. Probes were purified via a Zymo Oligo Clean and Concentrator kit (Zymo 4060), and eluate was diluted to ~12.5 µM DNA. All probes had >70% labeling efficiency and were used at a 1:100 dilution.

For IF alone, cells were fixed in 4% PFA as indicated, and simultaneously permeabilized and blocked for 10 min at room temperature in AbDil buffer (PBS with 6% BSA and 0.5% Triton X-100). Primary antibody incubations were in 0.5× AbDil in PBS for either 1 h at room temperature or overnight at 4°C. After washing in PBS, cells were incubated with secondary antibody in 0.5× AbDil for 1 h at room temperature, followed by washing in PBS, and epifluorescence microscopy done using either an EVOS M5000 fluorescence microscope or the Nikon Eclipse Ti2 microscope.

Quantification of smFISH images

A customized version of the Big-FISH python package (https://github.com/fish-quant/big-fish) (Imbert et al. 2022) was used to quantify mRNAs detected via smFISH in deconvolved images as described previously (Helton et al. 2025). In this analysis, the cytoplasm and stress granules are segmented based on GFP-G3BP1 or other stress granule marker intensity, nuclei are segmented based on Hoechst staining, and smFISH signal detected as spots. To account for variations in cell-to-cell brightness of the EGFP-G3BP1 stress granule marker, the ImageJ "localize normal intensity" function was applied to the green channel before detection of stress granules, nuclei, and cells via manual thresholding. We verified that the percent *AHNAK* mRNA in stress granules determined by hand using the Cell Counter tool in ImageJ/Fiji was not significantly different by automated quantification (Supplemental Fig. S1) and as reported previously in Helton et al. (2025).

Source data are reported in Supplemental Table S1.

SUPPLEMENTAL MATERIAL

Supplemental material is available for this article.

ACKNOWLEDGMENTS

We thank all members of the Moon Lab and Anthony Antonellis for helpful feedback. Figure 7 was made using BioRender.com.

This work was supported by National Institutes of Health grants R35GM146711 (S.L.M.) and K12GM111725 (M.B.).

Author contributions: Conceptualization: M.B., S.L.M.; data curation: M.B., B.D., S.L.M., N.S.H.; formal analysis: M.B., S.L.M., N.S.H.; funding acquisition: S.L.M., M.B.; investigation: M.B.; methodology: M.B., N.S.H., B.D., and S.L.M.; project administration: B.D., S.L.M.; resources: B.D., N.S.H., S.L.M.; software: N.S.H., M.B., S.L.M.; supervision: S.L.M.; validation: M.B.; visualization: M.B., S.L.M.; writing (original draft): M.B., S.L.M.; writing (editing): B.D., S.L.M.

Received November 29, 2025; accepted January 27, 2026.

REFERENCES

Antonellis A, Ellsworth RE, Sambuughin N, Puls I, Abel A, Lee-Lin S-Q, Jordanova A, Kremensky I, Christodoulou K, Middleton LT, et al. 2003. Glycyl tRNA synthetase mutations in Charcot-Marie-Tooth disease type 2D and distal spinal muscular atrophy type V. *Am J Hum Genet* **72:** 1293–1299. doi:10.1086/375039

Arimoto K, Fukuda H, Imajoh-Ohmi S, Saito H, Takekawa M. 2008. Formation of stress granules inhibits apoptosis by suppressing stress-responsive MAPK pathways. *Nat Cell Biol* **10:** 1324–1332. doi:10.1038/ncb1791

Aulas A, Lyons SM, Fay MM, Anderson P, Ivanov P. 2018. Nitric oxide triggers the assembly of "type II" stress granules linked to decreased cell viability. *Cell Death Dis* **9:** 1–14. doi:10.1038/s41419-018-1173-x

Azzam ME, Algranati ID. 1973. Mechanism of puromycin action: fate of ribosomes after release of nascent protein chains from polysomes. *Proc Natl Acad Sci* **70:** 3866–3869. doi:10.1073/pnas.70.12.3866

Baymiller M, Helton NS, Dodd B, Moon SL. 2026. tRNA synthetase activity is required for stress granule and P-body assembly. *Genes Dev* **40:** 475–497. doi:10.1101/gad.353535.125

Burke JM, Lester ET, Tauber D, Parker R. 2020. RNase L promotes the formation of unique ribonucleoprotein granules distinct from stress granules. *J Biol Chem* **295:** 1426–1438. doi:10.1074/jbc.RA119.011638

Costa-Mattioli M, Walter P. 2020. The integrated stress response: from mechanism to disease. *Science* **368:** eaat5314. doi:10.1126/science.aat5314

Darnell AM, Subramaniam AR, O'Shea EK. 2018. Translational control through differential ribosome pausing during amino acid limitation in mammalian cells. *Mol Cell* **71:** 229–243.e11. doi:10.1016/j.molcel.2018.06.041

Dever TE, Feng L, Wek RC, Cigan AM, Donahue TF, Hinnebusch AG. 1992. Phosphorylation of initiation factor 2α by protein kinase GCN2 mediates gene-specific translational control of *GCN4* in yeast. *Cell* **68:** 585–596. doi:10.1016/0092-8674(92)90193-G

Dieterich DC, Link AJ, Graumann J, Tirrell DA, Schuman EM. 2006. Selective identification of newly synthesized proteins in mammalian cells using bioorthogonal noncanonical amino acid tagging (BONCAT). *Proc Natl Acad Sci* **103:** 9482–9487. doi:10.1073/pnas.0601637103

Dong J, Qiu H, Garcia-Barrio M, Anderson J, Hinnebusch AG. 2000. Uncharged tRNA activates GCN2 by displacing the protein kinase moiety from a bipartite tRNA-binding domain. *Mol Cell* **6:** 269–279. doi:10.1016/S1097-2765(00)00028-9

Enam SU, Zinshteyn B, Goldman DH, Cassani M, Livingston NM, Seydoux G, Green R. 2020. Puromycin reactivity does not accurately localize translation at the subcellular level. *eLife* **9:** e60303. doi:10.7554/eLife.60303

Gaspar I, Wippich F, Ephrussi A. 2017. Enzymatic production of single-molecule FISH and RNA capture probes. *RNA* **23:** 1582–1591. doi:10.1261/rna.061184.117

Goldman DH, Livingston NM, Movsik J, Wu B, Green R. 2021. Live-cell imaging reveals kinetic determinants of quality control triggered by ribosome stalling. *Mol Cell* **81:** 1830–1840.e8. doi:10.1016/j.molcel.2021.01.029

Grollman AP. 1968. Inhibitors of protein biosynthesis. *J Biol Chem* **243:** 4089–4094. doi:10.1016/S0021-9258(18)93283-7

Guillén-Boixet J, Kopach A, Holehouse AS, Wittmann S, Jahnel M, Schlüßler R, Kim K, Trussina IREA, Wang J, Mateju D, et al. 2020. RNA-induced conformational switching and clustering of G3BP drive stress granule assembly by condensation. *Cell* **181:** 346–361.e17. doi:10.1016/j.cell.2020.03.049

Habibi D, Ogloff N, Jalili RB, Yost A, Weng AP, Ghahary A, Ong CJ. 2012. Borrelidin, a small molecule nitrile-containing macrolide inhibitor of threonyl-tRNA synthetase, is a potent inducer of apoptosis in acute lymphoblastic leukemia. *Invest New Drugs* **30:** 1361–1370. doi:10.1007/s10637-011-9700-y

Helton NS, Dodd B, Moon SL. 2025. Ribosome association inhibits stress-induced gene mRNA localization to stress granules. *Genes Dev* **39:** 826–848. doi:10.1101/gad.352899.125

Imbert A, Ouyang W, Safieddine A, Coleno E, Zimmer C, Bertrand E, Walter T, Mueller F. 2022. FISH-quant v2: a scalable and modular tool for smFISH image analysis. *RNA* **28:** 786–795. doi:10.1261/rna.079073.121

Inglis AJ, Masson GR, Shao S, Perisic O, McLaughlin SH, Hegde RS, Williams RL. 2019. Activation of GCN2 by the ribosomal P-stalk. *Proc Natl Acad Sci* **116:** 4946–4954. doi:10.1073/pnas.1813352116

Jin D, Wek SA, Kudlapur NT, Cantara WA, Bakhtina M, Wek RC, Musier-Forsyth K. 2021. Disease-associated mutations in a bifunctional aminoacyl-tRNA synthetase gene elicit the integrated stress response. *J Biol Chem* **297:** 101203. doi:10.1016/j.jbc.2021.101203

Jin D, Wek SA, Cordova RA, Wek RC, Lacombe D, Michaud V, Musier-Forsyth K. 2023. Aminoacylation-defective bi-allelic mutations in human EPRS1 associated with psychomotor developmental delay, epilepsy, and deafness. *Clin Genet* **103:** 358–363. doi:10.1111/cge.14269

Kedersha N, Cho MR, Li W, Yacono PW, Chen S, Gilks N, Golan DE, Anderson P. 2000. Dynamic shuttling of TIA-1 accompanies the recruitment of mRNA to mammalian stress granules. *J Cell Biol* **151:** 1257–1268. doi:10.1083/jcb.151.6.1257

Kedersha N, Stoecklin G, Ayodele M, Yacono P, Lykke-Andersen J, Fritzler MJ, Scheuner D, Kaufman RJ, Golan DE, Anderson P. 2005. Stress granules and processing bodies are dynamically linked sites of mRNP remodeling. *J Cell Biol* **169:** 871–884. doi:10.1083/jcb.200502088

Kedersha N, Panas MD, Achorn CA, Lyons S. 2016. G3BP–Caprin1–USP10 complexes mediate stress granule condensation and associate with 40S subunits. *J Cell Biol* **212:** 845–860. doi:10.1083/jcb.201508028

Keller TL, Zocco D, Sundrud MS, Hendrick M, Edenius M, Yum J, Kim Y-J, Lee H-K, Cortese JF, Wirth DF, et al. 2012. Halofuginone and other febrifugine derivatives inhibit prolyl-tRNA synthetase. *Nat Chem Biol* **8:** 311–317. doi:10.1038/nchembio.790

Khong A, Parker R. 2018. mRNP architecture in translating and stress conditions reveals an ordered pathway of mRNP compaction. *J Cell Biol* **217:** 4124–4140. doi:10.1083/jcb.201806183

Khong A, Matheny T, Jain S, Mitchell SF, Wheeler JR, Parker R. 2017. The stress granule transcriptome reveals principles of mRNA accumulation in stress granules. *Mol Cell* **68:** 808–820.e5. doi:10.1016/j.molcel.2017.10.015

Kuo ME, Antonellis A. 2020. Ubiquitously expressed proteins and restricted phenotypes: exploring cell-specific sensitivities to impaired tRNA charging. *Trends Genet* **36:** 105–117. doi:10.1016/j.tig.2019.11.007

Misra J, Holmes MJ, Mirek E T, Langevin M, Kim H-G, Carlson KR, Watford M, Dong XC, Anthony TG, Wek RC. 2021. Discordant regulation of eIF2 kinase GCN2 and mTORC1 during nutrient stress. *Nucleic Acids Res* **49:** 5726–5742. doi:10.1093/nar/gkab362

Misra J, Carlson KR, Spandau DF, Wek RC. 2024. Multiple mechanisms activate GCN2 eIF2 kinase in response to diverse stress conditions. *Nucleic Acids Res* **52:** 1830–1846. doi:10.1093/nar/gkae006

Mollet S, Cougot N, Wilczynska A, Dautry F, Kress M, Bertrand E, Weil D. 2008. Translationally repressed mRNA transiently cycles through stress granules during stress. *Mol Biol Cell* **19:** 4469–4479. doi:10.1091/mbc.e08-05-0499

Moon SL, Morisaki T, Khong A, Lyon K, Parker R, Stasevich TJ. 2019. Multicolour single-molecule tracking of mRNA interactions with RNP granules. *Nat Cell Biol* **21:** 162–168. doi:10.1038/s41556-018-0263-4

Moon SL, Morisaki T, Stasevich TJ, Parker R. 2020. Coupling of translation quality control and mRNA targeting to stress granules. *J Cell Biol* **219:** e202004120. doi:10.1083/jcb.202004120

Moutaoufik MT, El Fatimy R, Nassour H, Gareau C, Lang J, Tanguay RM, Mazroui R, Khandjian EW. 2014. UVC-induced stress granules in mammalian cells. *PLoS One* **9:** e112742. doi:10.1371/journal.pone.0112742

Pakos-Zebrucka K, Koryga I, Mnich K, Ljujic M, Samali A, Gorman AM. 2016. The integrated stress response. *EMBO Rep* **17:** 1374–1395. doi:10.15252/embr.201642195

Pietras P, Aulas A, Fay MM, Leśniczak-Staszak M, Sowiński M, Lyons SM, Szaflarski W, Ivanov P. 2022. Translation inhibition and suppression of stress granules formation by cisplatin. *Biomed Pharmacother* **145:** 112382. doi:10.1016/j.biopha.2021.112382

Pines M, Nagler A. 1998. Halofuginone: a novel antifibrotic therapy. *Gen Pharmacol* **30:** 445–450. doi:10.1016/S0306-3623(97)00307-8

Pitera AP, Szaruga M, Peak-Chew S-Y, Wingett SW, Bertolotti A. 2022. Cellular responses to halofuginone reveal a vulnerability of the GCN2 branch of the integrated stress response. *EMBO J* **41:** e109985. doi:10.15252/embj.2021109985

Rai S, Szaruga M, Pitera AP, Bertolotti A. 2024. Integrated stress response activator halofuginone protects mice from diabetes-like phenotypes. *J Cell Biol* **223:** e202405175. doi:10.1083/jcb.202405175

Sanders DW, Kedersha N, Lee DSW, Strom AR, Drake V, Riback JA, Bracha D, Eeftens JM, Iwanicki A, Wang A, et al. 2020. Competing protein-RNA interaction networks control multiphase intracellular organization. *Cell* **181:** 306–324.e28. doi:10.1016/j.cell.2020.03.050

Schindelin J, Arganda-Carreras I, Frise E, Kaynig V, Longair M, Pietzsch T, Preibisch S, Rueden C, Saalfeld S, Schmid B, et al. 2012. Fiji: an open-source platform for biological-image analysis. *Nat Methods* **9:** 676–682. doi:10.1038/nmeth.2019

Sidhu A, Miller JR, Tripathi A, Garshott DM, Brownell AL, Chiego DJ, Arevang C, Zeng Q, Jackson LC, Bechler SA, et al. 2015. Borrelidin induces the unfolded protein response in oral cancer cells and chop-dependent apoptosis. *ACS Med Chem Lett* **6:** 1122–1127. doi:10.1021/acsmedchemlett.5b00133

Sidrauski C, Acosta-Alvear D, Khoutorsky A, Vedantham P, Hearn BR, Li H, Gamache K, Gallagher CM, Ang KK-H, Wilson C, et al. 2013. Pharmacological brake-release of mRNA translation enhances cognitive memory. *eLife* **2:** e00498. doi:10.7554/eLife.00498

Sidrauski C, McGeachy AM, Ingolia NT, Walter P. 2015. The small molecule ISRIB reverses the effects of eIF2α phosphorylation on translation and stress granule assembly. *eLife* **4:** e05033. doi:10.7554/eLife.05033

Sinha NK, Ordureau A, Best K, Saba JA, Zinshteyn B, Sundaramoorthy E, Fulzele A, Garshott DM, Denk T, Thoms M, et al. 2020. EDF1 coordinates cellular responses to ribosome collisions. *eLife* **9:** e58828. doi:10.7554/eLife.58828

Snieckute G, Ryder L, Vind AC, Wu Z, Arendrup FS, Stoneley M, Chamois S, Martinez-Val A, Leleu M, Dreos R, et al. 2023. ROS-induced ribosome impairment underlies ZAKα-mediated metabolic decline in obesity and aging. *Science* **382:** eadf3208. doi:10.1126/science.adf3208

Spaulding EL, Hines TJ, Bais P, Tadenev ALD, Schneider R, Jewett D, Pattavina B, Pratt SL, Morelli KH, Stum MG, et al. 2021. The integrated stress response contributes to tRNA synthetase-associated peripheral neuropathy. *Science* **373:** 1156–1161. doi:10.1126/science.abb3414

Stoneley M, Harvey RF, Mulroney TE, Mordue R, Jukes-Jones R, Cain K, Lilley KS, Sawarkar R, Willis AE. 2022. Unresolved stalled ribosome complexes restrict cell-cycle progression after genotoxic stress. *Mol Cell* **82:** 1557–1572.e7. doi:10.1016/j.molcel.2022.01.019

Sundrud MS, Koralov SB, Feuerer M, Calado DP, Kozhaya AE, Rhule-Smith A, Lefebvre RE, Unutmaz D, Mazitschek R, Waldner H, et al. 2009. Halofuginone inhibits T_H17 cell differentiation by activating the amino acid starvation response. *Science* **324:** 1334–1338. doi:10.1126/science.1172638

Tsai JC, Miller-Vedam LE, Anand AA, Jaishankar P, Nguyen HC, Renslo AR, Frost A, Walter P. 2018. Structure of the nucleotide exchange factor eIF2B reveals mechanism of memory-enhancing molecule. *Science* **359:** eaaq0939. doi:10.1126/science.aaq0939

Wek RC, Jackson BM, Hinnebusch AG. 1989. Juxtaposition of domains homologous to protein kinases and histidyl-tRNA synthetases in GCN2 protein suggests a mechanism for coupling GCN4 expression to amino acid availability. *Proc Natl Acad Sci* **86:** 4579–4583. doi:10.1073/pnas.86.12.4579

Wu CC-C, Peterson A, Zinshteyn B, Regot S, Green R. 2020. Ribosome collisions trigger general stress responses to regulate cell fate. *Cell* **182:** 404–416.e14. doi:10.1016/j.cell.2020.06.006

Yang P, Mathieu C, Kolaitis R-M, Zhang P, Messing J, Yurtsever U, Yang Z, Wu J, Li Y, Pan Q, et al. 2020. G3BP1 is a tunable switch that triggers phase separation to assemble stress granules. *Cell* **181:** 325–345.e28. doi:10.1016/j.cell.2020.03.046

Ying S, Khaperskyy DA. 2020. UV damage induces G3BP1-dependent stress granule formation that is not driven by mTOR inhibition-mediated translation arrest. *J Cell Sci* **133:** jcs248310. doi:10.1242/jcs.248310

Young SK, Wek RC. 2016. Upstream open reading frames differentially regulate gene-specific translation in the integrated stress response. *J Biol Chem* **291:** 16927–16935. doi:10.1074/jbc.R116.733899

Zhou Y, Panhale A, Shvedunova M, Balan M, Gomez-Auli A, Holz H, Seyfferth J, Helmstädter M, Kayser S, Zhao Y, et al. 2024. RNA damage compartmentalization by DHX9 stress granules. *Cell* **187:** P1701–P1718. doi:10.1016/j.cell.2024.02.028

Zhou C, Zhang M, Murray J, Paulo J, Gygi S, Shao S, Whitman M, Keller T. 2025. GCN1 couples GCN2 to ribosomal state to initiate amino acid response pathway signaling. *Science* **390:** eads8728. doi:10.1126/science.ads8728

Zuko A, Mallik M, Thompson R, Spaulding EL, Wienand AR, Been M, Tadenev ALD, van Bakel N, Sijlmans C, Santos LA, et al. 2021. tRNA overexpression rescues peripheral neuropathy caused by mutations in tRNA synthetase. *Science* **373:** 1161–1166. doi:10.1126/science.abb3356

MEET THE FIRST AUTHOR

Max Baymiller

***Meet the First Author(s)* is an editorial feature within *RNA*, in which the first author(s) of research-based papers in each issue have the opportunity to introduce themselves and their work to readers of *RNA* and the RNA research community. Max Baymiller is the first author of this paper, "Tuning tRNA synthetase inhibition reveals parabolic induction of stress granules limited in size and RNA content." Max is currently a Visiting Professor of Molecular Biology and Biochemistry at Wesleyan University.**

What are the major results described in your paper, and how do they impact this branch of the field?

We found that interfering with translation elongation causes an atypical trend in the assembly of RNA condensates called stress granules. Whereas during a "normal" stress you find more granules the more stress you have, with tRNA synthetase inhibitors we saw that granules can only form at intermediate levels of stress. This suggests that the many other stressors which impair elongation will only assemble granules if cells can balance activation of stress with the amount of mRNA that remains with ribosomes.

What led you to study RNA or this aspect of RNA science?

I originally started working on RNA as a grad student because I was interested in the RNA world and the origin of life. I was particularly taken with the role of tRNA and rRNA in translation as relics of a time before the dominance of proteins. I had some excellent mentors in graduate school (Susan Martinis and Auinash Kalsotra) who exposed me to a more contemporary world of RNA, including its many connections to disease. That led me to Stephanie Moon's lab and learning about RNA in the cellular stress response.

What are some of the landmark moments that provoked your interest in science or your development as a scientist?

Reading Carl Sagan as a kid definitely feels like the start for me. My dad (a car salesman, not a scientist) had all of Sagan's books, and I think left them lying around for me to find on purpose. I got hooked on the sense of wonder Sagan conveyed, and the sheer enormity of the universe as he described it. I am still influenced by that experience today: As a teacher, I always try to find places where I can feel a sense of awe about the course topics and then let those feelings show to my students.

What are your subsequent near- or long-term career plans?

This semester I'm very excited to be teaching an upper-level elective course in RNA Biology at Wesleyan, along with a lab class where students get to do some real molecular biology research. In the near future, I'm looking forward to having a permanent position where I can keep working with students in the classroom and the lab. This includes working with undergraduates to follow up on some outstanding questions I have from this research published in *RNA*!

Tuning tRNA synthetase inhibition reveals parabolic induction of stress granules limited in size and RNA content

Max Baymiller, Noah S. Helton, Benjamin Dodd, et al.

RNA 2026 32: 870-884 originally published online February 8, 2026
Access the most recent version at doi:10.1261/rna.080883.125